

# Poly(amino acid)s-based star AIEgens for cell uptake with pH-response and chiral difference

Wenli Feng<sup>a</sup>, Guofeng Li<sup>a,\*</sup>, Lei Tao<sup>b</sup>, Yen Wei<sup>b</sup>, Xing Wang<sup>a,\*</sup>

<sup>a</sup> Beijing Laboratory of Biomedical Materials, Beijing University of Chemical Technology, Beijing 100029, PR China

<sup>b</sup> The Key Laboratory of Bioorganic Phosphorus Chemistry & Chemical Biology (Ministry of Education), Department of Chemistry, Tsinghua University, Beijing 100084, PR China

## ARTICLE INFO

### Keywords:

Aggregation-induced emission (AIE)  
Poly(amino acid)s  
pH-responsive  
Chirality  
Cell  
Uptake

## ABSTRACT

Chiral aggregation-induced emission luminogens (AIEgens) are the new-generation chiral sensors that regulate chiral signals from the molecular level to the macroscopic assembly. Expanding applications of chiral AIEgens and in-depth understanding of their chiral recognition in biological systems are meaningful. Herein, two star chiral AIEgens, consisting of tetraphenylethene (TPE) as core and poly(*N*-acryloyl-*L*(*D*) valine) (PLV or PDV) as arms, were precisely synthesized via atom transfer radical polymerization (ATRP) technique and named TPE-PLV and TPE-PDV. They possessed typical AIE characteristics and exhibited an increase in concentration-dependent fluorescence intensity. The two AIEgens were pH-responsive and had strong AIE-related emission in acidic solution. Importantly, AIEgens can enter the living cells by ATP dependent endocytosis, then light them up. The interactions between the AIEgens and living human hepatocarcinoma (HepG2) cells revealed that the internalization process of TPE-PLV and TPE-PDV was both chiral-dependent and pH-responsive. This novel strategy for synthesizing poly(amino acid)s functionalized AIEgens could inspire the development of promising fluorescent materials with chirality.

## 1. Introduction

Aggregation-induced emission (AIE) has attracted the continued attention since it was coined by Tang in 2001 [1]. Surpassing traditional organic fluorophores, the newly developed luminogens with AIE characteristics are becoming attractive candidates for advanced biosensing and imaging application [2,3]. Tetraphenylethylene (TPE), as a typical AIE luminogen (AIEgen), has been incorporated into polymers to visualize living cells, deliver drugs for tumor therapy due to its specific chemical and physical properties [4–6]. However, traditional AIEgens, such as TPE, are mostly non-planar molecular with poor water solubility, which limit their *in vivo* studies. Combination of AIEgens and nature biomolecules is a mature strategy that could overcome their intrinsic limitations including poor hydrophilicity, weak structural stability, and non-negligible biotoxicity [7,8].

Amino acid, as a natural chiral molecule, are vital components of life [9]. Over the past few years, amino acid-based polymers have been widely used in biological fields on account of their excellent biocompatibility, solubility in aqueous medium [10–14]. Wei and coworkers firstly synthesized AIE-active poly(amino acid)s nanoparticles that

display high water dispersibility, strong luminescence, and desirable biocompatibility [15]. Meanwhile, amino acid-based pendants in the synthetic polymers gave rise to stimuli-responsive properties such as pH, temperature, and ionic strength responses. Ding et al. discovered an AIE probe with the peptide incorporation, possessing much higher sensitivity in cancer cell targeting [16]. Tang and coworkers reported an *L*-leucine decorated AIEgen that exhibits a shortcut for the combination of AIE effect and chirality in the self-assemble structure [17]. The effects of chiral amino acids on AIEgens were widely studied. However, there was rarely reports to study chiral-specific interactions between bio-system and chiral AIEgens, regarding the fact that there is of pivotal interest in exploring the chirality-dependent cellular uptake and adsorption [18–20]. Therefore, the development of amino acid-based AIEgens for studying the chiral-specific interactions is promising, which allowed us to have a deeper understanding of the relationship between stereochemistry and cell uptake process.

Herein, two novel chiral AIEgens were prepared via integrating TPE with poly(*N*-acryloyl-*L*(*D*)-valine) by the atom transfer radical polymerization (ATRP) technique and named TPE-PLV and TPE-PDV (Scheme 1). Regardless of the typical AIE properties preserved by TPE-

\* Corresponding authors.

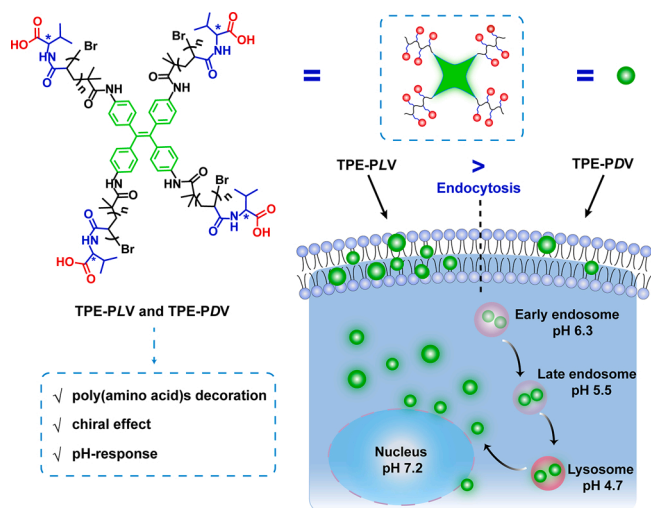
E-mail addresses: [chase.lg@163.com](mailto:chase.lg@163.com) (G. Li), [wangxing@mail.buct.edu.cn](mailto:wangxing@mail.buct.edu.cn) (X. Wang).

<https://doi.org/10.1016/j.colsurfb.2021.111687>

Received 2 November 2020; Received in revised form 1 March 2021; Accepted 7 March 2021

Available online 9 March 2021

0927-7765/© 2021 Published by Elsevier B.V.



**Scheme 1.** Cell uptake and imaging of pH-responsive chiral TPE-PLV and TPE-PDV star AIEgens.

PLV and TPE-PDV, the chiral valine-based polymer decorations further endowed them with good pH response, water solubility and biocompatibility. The highly emissive TPE-PLV and TPE-PDV can be internalized by living human hepatocarcinoma (HepG2) cells, and were selective for chirality and pH. Importantly, *in vitro* cell imaging suggested that these TPE-based chiral poly(amino acids) were promising for cell imaging and recognition, which has scarcely been reported in previous studies.

## 2. Experimental section

### 2.1. Materials

*L*-valine (99 %), *D*-valine (99 %), acryloyl chloride (97 %), 2-bromoisobutyryl bromide (98 %), triethylamine (TEA, 99 %), copper(I) bromide (CuBr, 99 %), ethylene diamine tetraacetic acid (EDTA, 99 %), 3-(4,5-dimethylazoloyl-2)-2,5-diphenyl tetrazolium bromide (MTT) were all purchased from Sigma-Aldrich and used as received. 1,1,2,2-tetrakis(4-aminophenyl) ethane (TPE-NH<sub>2</sub>, 97 %) was purchased from Energy Chemical and used as received. Ethyl acetate, anhydrous tetrahydrofuran (THF), and sodium sulfate (Na<sub>2</sub>SO<sub>4</sub>) were purchased from J&K Scientific. HepG2 cells were purchased from the Cell Resource Center, IBMS, CAMS/PUMC, Beijing, China. Dulbecco's modified Eagle's medium (DMEM), fetal bovine serum (FBS), penicillin, and streptomycin were purchased from Gibco BRL (Gaithersburg, MD, U.S.A.).

### 2.2. Characterizations

<sup>1</sup> Nuclear magnetic resonance (NMR) spectra were gained by the 'Bruker-Spectrospin' instrument (400 MHz) at room temperature using DMSO-*d*<sub>6</sub> and D<sub>2</sub>O as solvents. Gel permeation chromatography (GPC) was conducted with a Waters 1525 differential refractometer using THF as an eluent at 30 °C with a flow rate of 1 mL/min, calibrating with linear polystyrene standards. Ultraviolet-visible (UV-vis) absorption spectroscopy was recorded on UV/vis/NIR 2600 spectrometer (Shimadzu, Japan) with quartz cuvettes of 1 cm path length. Circular dichroism (CD) spectrum was recorded on CD spectrometer (J-815, JASCO) with quartz cuvettes of 10 mm path length. Fluorescence spectra (FL) were performed using an F-4600 spectrometer (Edinburgh, UK) with a slit width of 3 nm for both excitation and emission. Dynamic light scattering (DLS) was performed on a Zetasizer NanoZS (Malvern Instruments Ltd., Worcestershire, UK).

### 2.3. Synthesis of *N*-acryloyl-*L*(*D*)-valine monomers

*N*-acryloyl-*L*(*D*)-valine monomer was synthesized as reported previously [21]. In a typical procedure (e.g. synthesis of *N*-acryloyl-*L*-valine monomer): *L*-valine (2 g, 17.1 mmol) was dissolved in 5 mL of deionized water and subsequently added to acryloyl chloride (1.85 g, 20.5 mmol). After adding acryloyl chloride, the reaction was kept at 0 °C for 30 min, and then warmed up to room temperature for another 4 h. Then, the solution was extracted with ethyl acetate, and the organic phase was dried with anhydrous Na<sub>2</sub>SO<sub>4</sub>. After filtration and evaporation to obtain the colorless granular crystals with a yield above 85%. <sup>1</sup>H NMR (Fig. S1, 400 MHz, DMSO-*d*<sub>6</sub>, δ, ppm): 0.98 (CH(CH<sub>3</sub>)<sub>2</sub>, 9H, d), 1.90 (CH(CH<sub>3</sub>)<sub>2</sub>, 1H, m), 4.35 (CHCOO, 1H, d), 5.74-6.48 (CH = CH<sub>2</sub>, 3H, m), 8.38 (NH, 1H, s), 12.39 (COOH, 1H, s). <sup>13</sup>C NMR (Fig. S2, 600 MHz, DMSO-*d*<sub>6</sub>, δ, ppm): 172.93, 164.68, 131.31, 125.61, 57.18, 29.84, 19.10, 18.00. ESI-MS (Fig. S3) *m/z* calcd for (C<sub>8</sub>H<sub>13</sub>NO<sub>3</sub>): 171.09, found: ([M-H]<sup>-</sup>, 100%): 170.1.

### 2.4. Synthesis of 4-arm initiator (TPE-Br)

TPE-NH<sub>2</sub> (100 mg, 0.25 mmol) was dissolved in 17 mL of anhydrous THF. Then 2-bromoisobutyryl bromide (281.4 mg, 1.2 mmol) and TEA (424 μL, 3 mmol) was added with stirring. The reaction was kept at 0 °C for 1 h and then warmed up to room temperature for another 24 h. The mixture was washed with 1 M HCl for 1 time, NaHCO<sub>3</sub> for 2 times, NaCl for 1 time, respectively. The organic phase was dried with anhydrous Na<sub>2</sub>SO<sub>4</sub>. After filtration and evaporation to remove most of the solvent, the concentrated solution was further dried using a vacuum oven overnight. Then the mixture was treated by repeated centrifugal washing process for thrice by dissolving in ethanol, filtered, and precipitated into deionized water. And the organic phase was dried with anhydrous Na<sub>2</sub>SO<sub>4</sub>. After filtration and evaporation to remove most of the solvent, the concentrated solution was further dried using a vacuum oven overnight. The pure TPE-Br was stored at 4 °C for further use. <sup>13</sup>C NMR (Fig. S4, 400 MHz, DMSO-*d*<sub>6</sub>, δ, ppm): 169.66., 139.57, 139.52, 137.36, 131.60, 120.23, 61.24, 31.17. ESI-MS (Fig. S5) *m/z* calcd for (C<sub>42</sub>H<sub>44</sub>Br<sub>4</sub>N<sub>4</sub>O<sub>4</sub>): 988.01, found: ([M + Na]<sup>+</sup>, 100 %): 1011.109, ([M], 100 %): 988.112, ([M-Br + Na]<sup>+</sup>, 100 %): 931.182, ([M-Br], 100 %): 908.18, ([M-2Br + Na]<sup>+</sup>, 100 %): 851.245, ([M-2Br], 100 %): 826.246, ([M-3Br + Na]<sup>+</sup>, 100 %): 769.308, ([M-3Br], 100 %): 746.308, ([M-4Br + Na]<sup>+</sup>, 100 %): 687.366, ([M-4Br], 100 %): 664.368.

### 2.5. Synthesis of TPE-PLV and TPE-PDV

TPE-PV (abbreviation of TPE-PLV and TPE-PDV) was synthesized by the ATRP technique. A representative example of TPE-PLV is as follows. TPE-Br (10 mg, 0.01 mmol), *N*-acryloyl-*L*-valine monomer (688 mg, 4 mmol), 1 mL the mixed solvent of which the volume ratio is 2:1:1 of butanone, methanol, deionized water, respectively, were placed in a dry glass ampule equipped with a magnetic stir bar, and then the solution was degassed by sonication for 20 min. Then, CuBr (40 mg, 0.28 mmol) and PMDTEA (175 μL, 0.84 mmol) were added rapidly, and the obtained mixture was degassed by two freeze-evacuate-thaw cycles. The reaction vial was placed in a preheated reaction block at 60 °C for 4 h. The reaction was stopped by rapid cooling with liquid nitrogen. The reaction mixture was added EDTA (100 mg, 0.34 mmol), and its pH was maintained at 8 by the addition of 2 M NaOH. The above mixture was purified by dialysis against deionized water for 48 h using a dialysis membrane (molecular weight cut-off: 1000 Da). Fresh deionized water was replenished periodically. The dialyzed polymers were lyophilized and stored in dark conditions at 4 °C.

### 2.6. *In vitro* cytotoxicity assay

The cytotoxicity of TPE-PLV against HepG2 cells was evaluated in

vitro by methyl thiazolyl tetrazolium (MTT) assay. Briefly, the cells were plated in a 96-well plate (5000 cells per well) in 100  $\mu\text{L}$  DMEM medium supplemented with 10 % FBS, 100 units  $\text{mL}^{-1}$  penicillin, and 100  $\mu\text{g}$   $\text{mL}^{-1}$  streptomycin for 12 h. Then 10  $\mu\text{L}$  TPE-PLV at various concentrations in DMEM was added. The cells were cultured for 24 h and 48 h at 37  $^{\circ}\text{C}$  and the cell medium was replaced with fresh culture medium. Then, 20  $\mu\text{L}$  of MTT solution in PBS (5  $\text{mg}$   $\text{mL}^{-1}$ ) was added and incubated for another 4 h. The medium was aspirated, the MTT-formazan generated by live cells was dissolved in 150  $\mu\text{L}$  of DMSO, and the absorbance at a wavelength of 490 nm of each well was measured using a microplate reader. The relative cell viability (%) was determined by comparing the absorbance at 490 nm with control wells containing only cell culture medium.

## 2.7. Live cell imaging

HepG2 cells were first seeded in 20 mm diameter glass coverslips at the density of  $5 \times 10^4$  cells per well in cell culture medium and incubated with 10 % FBS, 100 units  $\text{mL}^{-1}$  penicillin and 100  $\mu\text{g}$   $\text{mL}^{-1}$  streptomycin in the humidified incubator of 95 % air and 5%  $\text{CO}_2$  at 37  $^{\circ}\text{C}$  for 12 h to allow cells attachment. Then, the cell culture was replaced with 1 mL fresh medium, which contained TPE-PLV or TPE-PDV (500  $\mu\text{g}$   $\text{mL}^{-1}$ ). After 24 h of incubation, cells were washed with PBS three times. Then the cell culture was treated with pH 4.56 and 7.92 no phenol red DMEM for 30 min. Subsequently, cell images were taken by a confocal laser scanning microscope (CLSM) Leica TCSSP8 3-channel (Leica, Germany) with the excitation wavelength of 405 nm. The fluorescence intensity was calculated using the free *Image J* software.

## 2.8. Flow cytometry study

HepG2 cells were seeded onto a 6-well plate ( $4 \times 10^5$  cells per well) and allowed to grow for 24 h. Then, the cell culture was replaced with 1 mL fresh medium, the cells were incubated 1 h at 37  $^{\circ}\text{C}$  and 4  $^{\circ}\text{C}$ , respectively. TPE-PLV was added to each dish (200  $\mu\text{g}$   $\text{mL}^{-1}$ ). After 6 h incubated, the cells were washed three times with PBS. After trypsin treatment, the cells were washed with PBS twice and then resuspended in 1 mL PBS. Fluorescence histograms were recorded with the BD FACSAriaSORP flow cytometer and analyzed using *Flowjo* software.

## 2.9. Cellular uptake assay

HepG2 cells were seeded onto 12-well plates ( $1 \times 10^6$  cells per well) for 24 h incubation. Then, the cell culture was replaced with 1 mL fresh medium which contained different concentration of TPE-PLV or TPE-PDV (160 and 500  $\mu\text{g}$   $\text{mL}^{-1}$ ) and further incubated for 24 h at 37  $^{\circ}\text{C}$  in 5%  $\text{CO}_2$  incubator. After washed with PBS three times, cells were lysed with 0.5 % Triton X-100 in 0.2 M NaOH solution (0.5 mL). The fluorescence intensity of the lysates was quantified using fluorescence microplate reader.

## 2.10. Statistical analysis

The experimental data are expressed as mean  $\pm$  standard deviation, and the significant difference between groups was analyzed using two-way ANOVA in Origin software. The statistical significance was set as ns  $p > 0.05$ , \*  $p < 0.05$ , \*\*  $p < 0.01$  and \*\*\*  $p < 0.001$ , respectively.

## 3. Results and discussion

### 3.1. Synthesis and characterization of TPE-PLV and TPE-PDV

Star AIEgens, TPE-PLV and TPE-PDV, were synthesized via a typical ATRP method (Scheme S1, Supporting Information). The stacked  $^1\text{H}$  NMR spectra (Fig. 1A) of TPE- $\text{NH}_2$ , TPE-Br, TPE-PLV, and TPE-PDV were recorded for comparison. To begin with, the 4-arm initiator TPE-Br was prepared by the amidation reaction. The new peak at around  $\delta$  1.9 ppm, which was attributed to the protons on the bromoisobutryl group, had an integration ratio of 6:4 when comparing with the aromatic ring ( $\delta$  7–8 ppm), suggesting successful synthesis of TPE-Br. In terms of the TPE-PLV and TPE-PDV, two peaks appeared at  $\delta$  0.9 ppm and  $\delta$  4 ppm were the evidence of the successful propagation of valine monomers (Fig. 1A). According to the peak integration ratio between the  $-\text{CH}_3$  group of valine units (peak a–b) and the phenyl group of TPE (peak i–l), there were around 13 units on each arm of the TPE-PLV and TPE-PDV. Further, the molecular weight ( $M_w$ ) calculated by the  $^1\text{H}$  NMR was around 9890  $\text{g mol}^{-1}$  for both oligomers, which was in good agreement with the molecular weight gained from GPC analysis (Fig. S6). Additionally, low dispersity of the two oligomers (1.11 for TPE-PLV, and 1.10

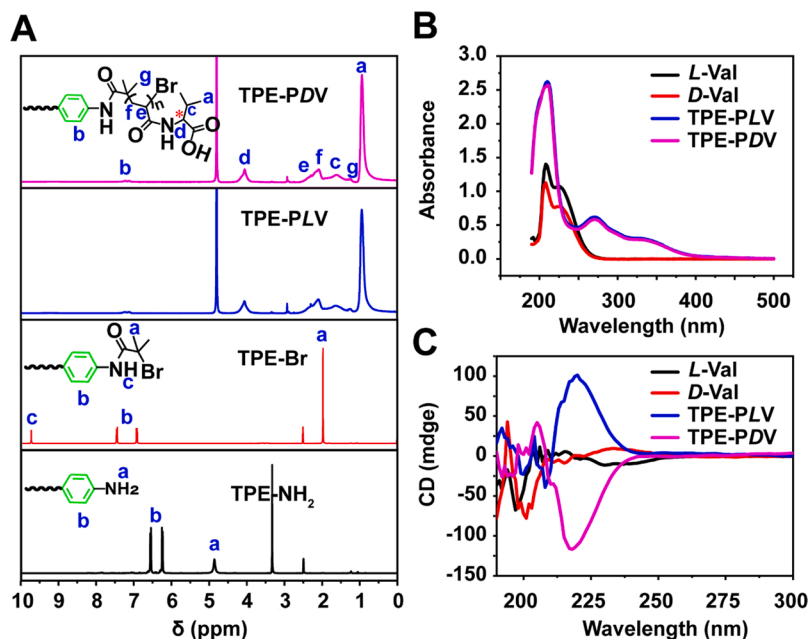


**Fig. 1.** Characterizations of TPE-PLV and TPE-PDV. (A) Stacked  $^1\text{H}$  NMR spectra (400 MHz) of TPE- $\text{NH}_2$ , TPE-Br ( $\text{DMSO}-d_6$ ), and TPE-PLV, TPE-PDV ( $\text{D}_2\text{O}$ ). (B) UV-vis absorption and (C) CD spectra of *N*-acryloyl-*L*-valine, *N*-acryloyl-*D*-valine, TPE-PLV, and TPE-PDV.

for TPE-PDV, Table S1) suggested a robust control of the ATRP protocol for the polymerization of *N*-acryloyl-L(D)-valine monomers. All these results indicated that both of the TPE-PLV and TPE-PDV had similar  $M_w$  and dispersity. As a result, it was in favor of studying the chiral effect on the physical and chemical properties of amino acid-based polymers under the same condition (Scheme 1).

### 3.2. Optical property

The optical properties of TPE-PLV and TPE-PDV were investigated. The UV-vis spectra of *N*-acryloyl-L(D)-valine, TPE-PLV, and TPE-PDV in water were given in Fig. 1B. After polymerization, the absorption peak of -COOH group in TPE-PV was shifted from 205 nm to 210 nm and the intensity increased significantly. Meanwhile, the absorption peak of the double bond on the monomer at 230 nm disappeared. The new peak located at 325-375 nm, corresponding to the TPE unit in TPE-PV, was associated with  $\pi-\pi^*$  transition of the molecule. Moreover, the opposite CD traces (Fig. 1C) between 200 and 225 nm of TPE-PLV and TPE-PDV had revealed that the two oligomers possess an overall opposite stereochemistry due to the two chiral monomers applied. This difference was further amplified thanks to the high density of the amino acid-based pendants along the main chain built by the radical propagation technique. TPE-PV exhibited obvious fluorescence properties. Take TPE-PLV as an example, the emission wavelength of it was peaked at around 480 nm and the peak of the excitation wavelength was around 290 nm (Fig. S7A). Under UV ( $\lambda_{\text{ex}} = 400$  nm) irradiation, TPE-PLV and TPE-PDV showed almost the same fluorescence intensity (Fig. S7B).

### 3.3. AIE properties

TPE decorated with polymers can form a highly delocalized  $\pi-\pi$  conjugated backbone structure and show typical AIE characteristics [22]. TPE-PV were found has weak solubility in ethanol and excellent water solubility (Fig. S8). To investigate the AIE property of TPE-PV, we

monitored the emission of TPE-PV in water/ethanol mixtures (100  $\mu\text{M}$ , Fig. S9). The TPE-PV was highly soluble in water due to the PV chain, and showed a weak emission. Fluorescence intensity greatly enhanced when the ethanol fraction became higher in ethanol-water mixtures, demonstrating typical AIE features. For water-soluble AIEgens, concentration-dependent fluorescence intensity was used to prove its AIE property [23–25]. Additionally, the emission of TPE-PV in various concentration in water was also investigated. In a diluted solution (< 10  $\mu\text{M}$ ), TPE-PLV has weak emission ( $\lambda_{\text{ex}} = 400$  nm,  $\lambda_{\text{em}} = 492$  nm) because polymer chains were in an isolated state which increase the active intramolecular rotations of its aromatic rings (Fig. 2A). At low concentrations, the fluorescence intensity slowly increased along with the increase of concentration from 10 to 50  $\mu\text{M}$ . Whereas, the fluorescence intensity had been witnessed an exponential growth as the concentration was continuously increased from 50  $\mu\text{M}$  to higher values. Finally, when the concentration reached 500  $\mu\text{M}$ , the fluorescence intensity of TPE-PLV ( $\lambda_{\text{ex}} = 400$  nm,  $\lambda_{\text{em}} = 496$  nm) was 11-fold stronger than that of the concentration at 10  $\mu\text{M}$ . A similar phenomenon was observed from a corresponding photo of the samples in different concentrations (the inset in Fig. 2A). For TPE-PV, they would be a core-shell structure in water with TPE as the core and PV chains as the shell. According to the fluorescence spectra, it was extrapolated that the critical aggregation concentration (CAC) of TPE-PLV was  $\sim 65$   $\mu\text{M}$  (Fig. 2C). Nano-aggregates would form when the concentration above CAC [26,27]. The concentration-induced hydrodynamic diameter ( $D_h$ ) enhancement was supplemental evidence for the aggregation of the TPE-PLV (the red line in Fig. 2C). Meanwhile, there was a slight red-shift of maxima emission from 492 nm to 496 nm with increased concentration as the presence of aggregation which could lead to the formation of space conjugated structures [28]. In the aggregated states, the rotation of aromatic rings was inhibited due to the presence of  $\pi-\pi$  stacking and the restriction of intramolecular rotation or vibration [29,30]. Additionally, PLV decoration could provide steric hindrance to TPE. The abundant carboxyl groups (-COOH) in PLV promoted the formation of hydrogen bonds.

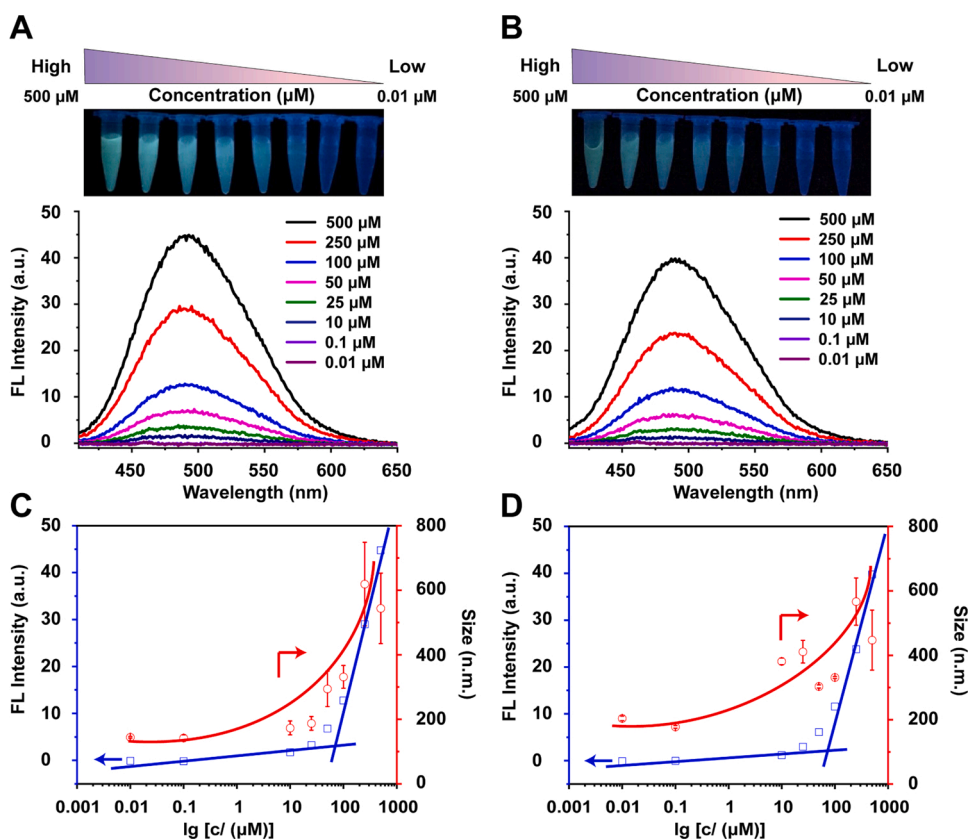


**Fig. 2.** AIE features of TPE-PLV and TPE-PDV. Concentration-dependent fluorescence spectra ( $\lambda_{\text{ex}} = 400$  nm) of (A) TPE-PLV and (B) TPE-PDV in water. The insets show images of TPE-PLV and TPE-PDV solutions with different concentrations ( $\mu\text{M}$ ) under 365 nm UV illumination. The critical aggregation concentration was determined by the fluorescence intensity versus the log concentration (blue) and hydrodynamic diameter (red) of (C) TPE-PLV and (D) TPE-PDV in water with different concentrations ( $\mu\text{M}$ ).

They further restricted molecular rotations and weakened the non-radiative transition of the chromophore, resulting in the fluorescence emission enhancement. Similar visible changes in the photoluminescence intensity were observed for TPE-PDV (Fig. 2B). The CAC of TPE-PDV was also  $\sim 65 \mu\text{M}$  (Fig. 2D). Overall, the differences in the emission of TPE-PDV and TPE-PLV at the same concentrations were negligible.

### 3.4. pH-Responsive

Benefiting from inherent carboxylic acid pendant groups, TPE-PV was capable of accepting protons at acid conditions, whereas releasing protons at alkaline conditions. It, thus, led to pH-responsive emission [31]. Take the TPE-PLV as an example, its fluorescence intensity was very low ( $\lambda_{\text{ex}} = 400 \text{ nm}$ ,  $\lambda_{\text{em}} = 460 \text{ nm}$ ) at pH 11.62, suggesting that it was highly soluble (Fig. 3A). As the pH of the solution was decreased all the way to 5.13, only a slight change of the fluorescence signal can be observed (Fig. 3A). Interestingly, further decrease of pH had resulted in a distinct increase of the fluorescence intensity. As shown, the intensity at pH 4.09 ( $\lambda_{\text{ex}} = 400 \text{ nm}$ ,  $\lambda_{\text{em}} = 480 \text{ nm}$ ) was about 30 times higher than that at pH 11.62 (Fig. 3C). Further decrease pH to 3.14, the fluorescent intensity of TPE-PLV ( $\lambda_{\text{ex}} = 400 \text{ nm}$ ,  $\lambda_{\text{em}} = 460 \text{ nm}$ ) was about 5-fold higher than that of the pH at 4.09. The blue-shifted emission from 480 nm to 460 nm could be attributed to the decreased electron-giving capacity of the carboxyl group. The fluorescence photos of the TPE-PLV solutions in the inset confirmed the trend of fluorescence intensity. The  $D_h$  of TPE-PLV was further measured to understand the effect of pH on the aggregation and fluorescence intensity. The average nano-aggregation size of TPE-PLV was constant at 200 nm when the pH values are ranging from 11.62 to 4.09 (Fig. S10A). Adjusting solution pH to 3.14 resulted in the increase of particle sizes (2500 nm), which restricted in their molecular motion and resulted in the stronger emission. Similar results were also observed between the fluorescence emission of TPE-PDV at various pH conditions (Fig. 3B and S10B), demonstrating the TPE-PLV and TPE-PDV possessed similar

pH-responsive emission. There were differences in that the size of TPE-PDV is slightly smaller than that of TPE-PLV in an acidic environment. It could be acceptable because most of the  $-\text{COOH}$  groups in TPE-PV were non-dissociative in acidic solution. TPE-PV randomly bonded to each other by hydrogen bond. Thus, the size of TPE-PV aggregates would distribute widely.

The emission enhancement could be a pH-driven switching the deprotonation equilibrium [32]. At  $\text{pH} < 5.00$ , most of the  $-\text{COOH}$  groups in TPE-PV were non-dissociative and bonded to each other with an intramolecular six-membered cyclic hydrogen bond [7]. Meanwhile, the TPE-PV turned more hydrophobic and the electrostatic attraction of the  $-\text{COOH}$  groups also became stronger, thus, leading to the aggregation of polymers. These small aggregates restricted its intramolecular rotation and resulted in emission enhancement (Fig. 3D). Whereas, at  $\text{pH} \geq 5.00$ , the  $-\text{COOH}$  deprotonated and ruptured the existing hydrogen bonds, and the electrostatic repulsion of  $-\text{COO}^-$  and chain conformation caused the dispersion of TPE-PV [33,34], thereby disintegrating the large aggregates into smaller aggregates. Overall, TPE-PV was pH-responsive and had strong AIE-related emission in acidic aqueous solution.

### 3.5. Intracellular imaging of chiral and pH-Responsive studies

TPE-PV can be utilized as visible materials to trace the interaction of chiral polymers and biosystems. *In vitro* cytotoxicity assay indicated TPE-PLV had a low cytotoxicity [35]. The cell viability was about 90 % and 78 % after 24 h of incubation with 160 and 500  $\mu\text{g mL}^{-1}$  TPE-PLV, respectively (Fig. S11). To investigate chiral-specific interactions between TPE-PV and cells, the endocytosis of TPE-PV was evaluated by confocal microscopy. Green fluorescence was observed in the cytoplasmic region for the cells treated with TPE-PV at pH 7.92 (Fig. 4A). In comparison with TPE-PDV, fluorescence intensity of TPE-PLV was ca. 1.25 times (t-test,  $p < 0.01$ , Fig. 4B), which testified TPE-PLV was more internalized by HepG2 cells. To further verify the chirality-dependent cellular uptake, the fluorescence intensity of cell lysates was detected

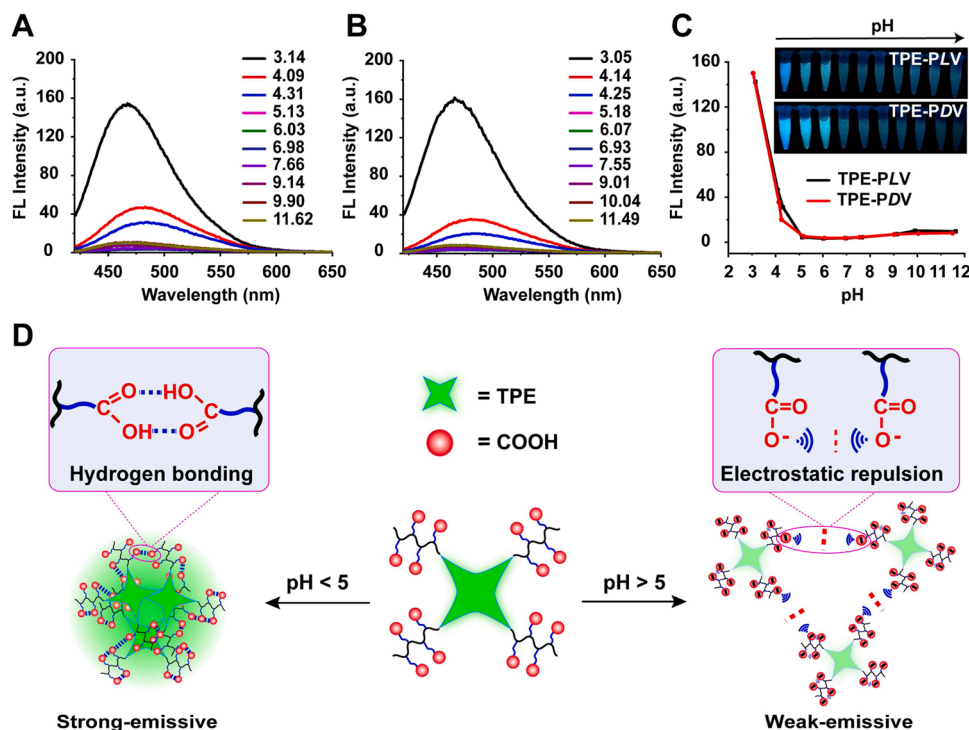


**Fig. 3.** pH-response induced AIE features. The fluorescence spectra ( $\lambda_{\text{ex}} = 400 \text{ nm}$ ) of (A) TPE-PLV and (B) TPE-PLV in water with different pH conditions. (C) The fluorescence intensity curves of TPE-PLV and TPE-PDV. The inset shows the emission images of the TPE-PLV and TPE-PDV solution in water with different pH conditions, respectively. (365 nm UV illumination) (D) Illustration of pH-responsive AIE effect of TPE-PV.

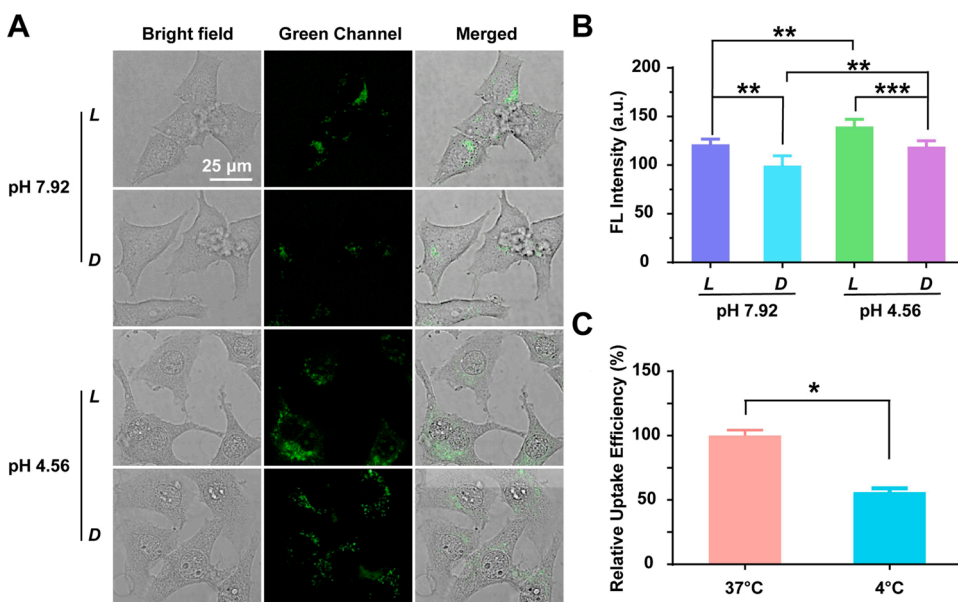


**Fig. 4.** *In vitro* evaluation of intracellular uptake TPE-PV. (A) CLSM images of HepG2 cells incubated with TPE-PLV and TPE-PDV ( $500 \mu\text{g mL}^{-1}$ ) under  $\text{pH} = 7.92$  and  $4.56$  in the dark at  $37 \text{ }^\circ\text{C}$ .  $\lambda_{\text{ex}} = 405 \text{ nm}$ . Scale bar,  $25 \mu\text{m}$ . (B) Statistical graph of fluorescence intensity counted by *image J* software ( $n = 6$ ; \*\* and \*\*\* denote significant difference at  $p < 0.01$  and  $p < 0.001$  levels, respectively; t-test). (C) Quantitative analysis of relative uptake efficiency of HepG2 cells pretreated with different temperatures for 24 h was determined by flow cytometry. \* indicates significant differences ( $p < 0.05$ ) compared with the  $37 \text{ }^\circ\text{C}$  group.

(Fig. S12). TPE-PLV showed significantly higher fluorescence intensity than TPE-PDV no matter at  $160 \mu\text{g mL}^{-1}$  (1.35 times, t-test,  $p < 0.01$ ) condition or  $500 \mu\text{g mL}^{-1}$  (1.36 times, t-test,  $p < 0.001$ ). The results confirmed TPE-PV has a chirality-dependent cellular uptake, which was in agreement with the previous studies [36–43]. Interestingly, different from chiral organic polymers, inorganic nanoparticles with *D*-configuration were easier internalized than *L*-configuration. This could be due to different cellular uptake mechanisms of organic polymers and inorganic nanoparticles. It was reported that the phospholipids and cholesterol on the cell membrane could affect the adhesion behavior of different chiral materials [44]. Additionally, there were specific receptors or biomolecules in cells could recognize *D*-configuration inorganic nanoparticles [45]. Taken together, there was no universal mechanisms explaining the internalization of different nanoparticles, but all these mechanisms were related to the process of cellular uptake [46]. Lowering the temperature is the common method to investigate ATP-dependent endocytosis of NPs [47,48]. When cells were cooled from  $37 \text{ }^\circ\text{C}$  to  $4 \text{ }^\circ\text{C}$ , there was an inhibition of the internalization of the capsule which is essential for ATP-dependent endocytosis [49]. Accordingly, the pathway for TPE-PV uptake was studied by flow cytometer under different temperatures [50,51]. It was found that when the temperature decreases, the amount of TPE-PLV entering the cell is significantly reduced ( $p < 0.05$ ). Meanwhile, there was no statistical difference in the fluorescence intensity of TPE-PLV at different temperatures without cells (Fig. S13). It was suggested the internalization process of TPE-PLV was ATP dependent endocytosis (Fig. 4C).

In further, TPE-PV could be utilized as a pH-responsive AIEgen for the detection of cellular uptake. Extracellular materials, including a variety of molecules, carriers and nanoparticles, are internalized by cells through endocytosis [52]. Once endocytosed, they encountered a gradient pH from early endosomes ( $\text{pH} 6.0\text{--}6.5$ ) and late endosomes ( $\text{pH} 5.0\text{--}6.0$ ) to lysosomes ( $\text{pH} 4.0\text{--}4.5$ ) [3]. It is an acceptable method to mimic endosomes by examining the pH-dependent emission by equilibrating intra- and extracellular pH [53,54]. Accordingly, to check the pH-dependent cell imaging of TPE-PV, the cells, which were pre-incubated with the TPE-PV at  $\text{pH} 7.92$ , were switched to  $\text{pH} 4.56$  medium for mimicking the lysosomes ( $\text{pH} 4.0\text{--}4.5$ ) [55,56]. TPE-PV, regardless of the chirality, exhibited enhanced fluorescence intensity at  $\text{pH} 4.56$  (Fig. 4A), which was 1.2 times than at  $\text{pH} 7.92$ , showing a pH-dependent increase in green fluorescence intensity (Fig. 4B). Different pH values would change the chain conformation, further affecting the AIEgen aggregation [57]. When the pH is  $7.92$ , the charge

density and hydrophilicity of the TPE-PV increased. The electrostatic repulsion between the chains caused the PV decoration adapt to a more extended conformation. Then the water molecules could close to the luminophore to produce non-radiative inactivation and reduce fluorescence. Furthermore, the intramolecular rotation of the TPE phenyl group cannot be completely stopped through the rotational energy relaxation channel. The entire molecule was in an excited state, leading to weak fluorescence. When the pH was lowered to  $4.56$ , the polymer chains part of the TPE-PV was protonated. The chains changed from partially charged to an uncharged state [58]. The polymer chains were contracted to prevent the contact between the phenyl ring and the water molecule, resulting in weak non-radiation inactivation and the fluorescence was enhanced. Meanwhile, the highly distorted molecular conformation produced a large amount of preferable intermolecular  $\pi\text{-}\pi$  stacking forces, thereby restricting the intramolecular rotation of the phenyl ring to a large extent and leading to increased fluorescence. The intracellular fluorescence changes afforded the strong evidence that TPE-PV was both chirality-dependent and pH-responsive.

TPE-PV is a versatile chiral AIEgens that processes multiple responsiveness. Nevertheless, TPE-PV may possess other potential properties that further broaden its applications. For example, using chiral induction effect and hydrogen bond interaction to precisely control the morphology of TPE-PV, which may introduce specific features [59–61]. It was demonstrated that radical amphiphilicity AMPs exhibited high antibacterial activity and low hemolytic activity by contrast to the typical facial amphiphilicity AMPs [62]. In addition, cellular internalized of supramolecular unfoldable single-chain nanogels (SCNGs) with high siRNAs delivery efficiency than non-unfoldable SCNGs [63]. That may be another direction for developing the multifunctional poly(amino acid)-based AIEgens.

#### 4. Conclusion

In summary, a handy method for preparing TPE based chiral poly(amino acid)s star AIEgens via ATRP was reported. The water-soluble TPE-PLV and TPE-PDV have typical AIE features and show an increase in concentration-dependent fluorescent intensity. TPE-PV was pH-responsive, and its fluorescence intensity showed an exponential enhance when  $\text{pH} < 5.0$ . More importantly, TPE-PV can be easily taken into cells by ATP dependent endocytosis, thus, light up the living cells. The internalization process of TPE-PV was chirality-dependent and pH-responsive, making it promising for bioimaging applications. We

believe this star chiral AIEgens could be a promising development for exploring the chiral effect between nanomaterials and biosystems.

### Data availability

The authors are unable or have chosen not to specify which data has been used.

### CRedit authorship contribution statement

**Wenli Feng:** Investigation, Software, Formal analysis, Data curation, Writing - original draft. **Guofeng Li:** Conceptualization, Supervision, Validation, Visualization, Writing - review & editing. **Lei Tao:** Conceptualization, Writing - review & editing. **Yen Wei:** Conceptualization, Resources, Writing - review & editing. **Xing Wang:** Conceptualization, Supervision, Funding acquisition, Writing - review & editing, Validation, Visualization.

### Declaration of Competing Interest

The authors declare no competing financial interest.

### Acknowledgments

X. W. thanks the National Natural Science Foundation (21574008) and the Fundamental Research Funds for the Central Universities (BHYC1705B) of China for their financial support.

### Appendix A. Supplementary data

Supplementary material related to this article can be found, in the online version, at doi:<https://doi.org/10.1016/j.colsurfb.2021.111687>.

### References

- J. Luo, Z. Xie, J.W.Y. Lam, L. Cheng, H. Chen, C. Qiu, H.S. Kwok, X. Zhan, Y. Liu, D. Zhu, B.Z. Tang, *Chem. Commun. (Camb.)* 18 (2001) 1740.
- S.S. Liow, H. Zhou, S. Sugiarto, S. Guo, M.L.S. Chalasani, N.K. Verma, J. Xu, X. J. Loh, *Biomacromolecules* 18 (2017) 886.
- Y. Cai, C. Gui, K. Samedov, H. Su, X. Gu, S. Li, W. Luo, H.H.Y. Sung, J.W.Y. Lam, R. T.K. Kwok, I.D. Williams, A. Qin, B.Z. Tang, *Chem. Sci.* 8 (2017) 7593.
- D.D. La, S.V. Bhosale, L.A. Jones, S.V. Bhosale, *ACS Appl. Mater. Interfaces* 10 (2017) 12189.
- B. Situ, X. Ye, Q. Zhao, L. Mai, Y. Huang, S. Wang, J. Chen, B. Li, B. He, Y. Zhang, J. Zou, B.Z. Tang, X. Pan, L. Zheng, *Adv. Sci.* 7 (2020), 1902760.
- Y. Zhao, Y. Wu, S. Chen, H. Deng, X. Zhu, *Macromolecules* 51 (2018) 5234.
- Z. Dong, H. Cui, Y. Wang, C. Wang, Y. Li, C. Wang, *Carbohydr. Polym.* 227 (2020), 115338.
- X. Shi, C.Y.Y. Yu, H. Su, R.T.K. Kwok, M. Jiang, Z. He, J.W.Y. Lam, B.Z. Tang, *Chem. Sci.* 8 (2017) 7014.
- I. Cobo, M. Li, B.S. Sumerlin, S. Perrier, *Nat. Mater.* 14 (2015) 143.
- I. Irwansyah, Y.Q. Li, W. Shi, D. Qi, W.R. Leow, M.B. Tang, S. Li, X. Chen, *Adv. Mater.* 27 (2015) 648.
- W. Shen, P. He, C. Xiao, X. Chen, *Adv. Healthcare Mater.* 7 (2018), 1800354.
- H. Sun, Y. Hong, Y. Xi, Y. Zou, J. Gao, J. Du, *Biomacromolecules* 19 (2018) 1701.
- C. Zheng, X.G. Zhang, L. Sun, Z.P. Zhang, C.X. Li, *J. Mater. Sci. Mater. Med.* 24 (2013) 931.
- Q. Gao, T. Feng, D. Huang, P. Liu, P. Lin, Y. Wu, Z. Ye, J. Ji, P. Li, W. Huang, *Biomater. Sci.* 8 (2020) 278.
- J. Tian, R. Jiang, P. Gao, D. Xu, L. Mao, G. Zeng, M. Liu, F. Deng, X. Zhang, Y. Wei, *Mat. Sci. Eng.: C* 79 (2017) 563.
- A. Han, H. Wang, R.T. Kwok, S. Ji, J. Li, D. Kong, B.Z. Tang, B. Liu, Z. Yang, D. Ding, *Anal. Chem.* 88 (2016) 3872.
- H. Li, J. Cheng, H. Deng, E. Zhao, B. Shen, J.W.Y. Lam, K.S. Wong, H. Wu, B.S. Li, B.Z. Tang, *J. Mater. Chem. C Mater. Opt. Electron. Devices* 3 (2015) 2399.
- X. Wang, H. Gan, T. Sun, *Adv. Fun. Mater.* 21 (2011) 3275.
- G.F. Liu, D. Zhang, C.L. Feng, *Angew. Chem. Int. Ed.* 53 (2014) 7789.
- X. Wang, X. Wang, M. Wang, D. Zhang, Q. Yang, T. Liu, R. Lei, S. Zhu, Y. Zhao, C. Chen, *Small* 14 (2018), 1703982.
- G. Li, W. Feng, N. Corrigan, C. Boyer, X. Wang, J. Xu, *Polym. Chem.* 9 (2018) 2733.
- S.W. Thomas, G.D. Joly, T.M. Swager, *Chem. Rev.* 107 (2007) 1339.
- Z. Wang, L. Yang, Y. Liu, Y. Liu, X. Huang, F. Qiao, W. Qim, Q. Hu, B.Z. Tang, *J. Mater. Chem. B Mater. Biol. Med.* 5 (2017) 4981.
- Z. Dong, Y. Bi, H. Cui, Y. Wang, C. Wang, Y. Li, H. Jin, C. Wang, *ACS Appl. Mater. Interfaces* 11 (2019) 23840.
- T. Xue, K. Shao, J. Xiang, X. Pan, Z. Zhu, Y. He, *Nanoscale* 12 (2020) 7509.
- N. Hao, C. Sun, Z. Wu, L. Xu, W. Gao, J. Cao, L. Li, B. He, *Bioconjugate Chem.* 28 (2017) 1944.
- Y. Xia, L. Dong, Y. Jin, S. Wang, L. Yan, S. Yin, S. Zhou, B. Song, *J. Mater. Chem. B Mater. Biol. Med.* 3 (2015) 491.
- L. Fang, C. Huang, G. Shabir, J. Liang, Z. Liu, H. Zhang, *ACS Macro Lett.* 8 (2019) 1605.
- B. Saha, B. Ruidas, S. Mete, C.D. Mukhopadhyay, K. Bauri, P. De, *Chem. Sci.* 11 (2020) 141.
- Z. Yang, W. Qin, N.L.C. Leung, M. Arseneault, J.W.Y. Lam, G. Liang, H.H.Y. Sung, I. D. Williams, B.Z. Tang, *J. Mater. Chem. C Mater. Opt. Electron. Devices* 4 (2016) 99.
- Y. Tang, Q. Wang, L. Wu, K. Liu, W. Wang, Y. Shen, Y. Xue, S. Dai, *React. Funct. Polym.* (2020), 104544.
- H. Guo, X. Cheng, H. Li, J. Li, J. Wei, C. Feng, *RSC Adv.* 10 (2020) 23532.
- X. Guan, D. Zhang, L. Meng, Y. Zhang, T. Jia, Q. Jin, Q. Wei, D. Lu, H. Ma, *Ind. Eng. Chem. Res.* 56 (2017) 680.
- F. Chen, C. Li, X. Wang, G. Liu, G. Zhang, *Soft Matter* 8 (2012) 6364.
- G. Li, H. Zhao, J. Hong, K. Quan, Q. Yuan, X. Wang, *Colloids Surf. B Biointerfaces* 160 (2017) 220.
- X. Wang, H. Gan, T. Sun, B. Su, H. Fuchs, D. Vestweber, S. Butz, *Soft Matter* 6 (2010) 3851.
- X. Yao, Y. Hu, B. Cao, R. Peng, J. Ding, *Biomaterials* 34 (2013) 9001.
- F. Zhou, L. Yuan, D. Li, H. Huang, T. Sun, H. Chen, *Colloids Surf. B Biointerfaces* 90 (2012) 97.
- W.P.R. Verdurmen, P.H. Bovee-Geurts, P. Wadhvani, A.S. Ulrich, M. Hallbrink, T. H. Van Kuppevelt, R. Brock, *Chem. Biol.* 18 (2011) 1000.
- I.E. Palamà, F.D. Maria, M. Zangoli, S. D'Amone, G. Manfredi, J. Barsotti, G. Lanzani, L. Ortolani, E. Salatelli, G. Gigli, G. Barbarella, *RSC Adv.* 9 (2019) 23036.
- N.N. Zhang, H.R. Sun, S. Liu, Y.C. Xing, J. Lu, F. Peng, C.L. Han, Z. Wei, T. Sun, B. Yang, K. Liu, *ACS Chem* (2021) 1.
- K. Hu, W. Li, M. Yu, C. Sun, Z. Li, *Bioconjugate Chem.* 27 (2016) 2824.
- A. Motealleh, H. Hermes, J. Jose, N.S. Kehr, *Nanomedicine (N. Y., NY, U. S.)* 14 (2018) 247.
- J. Yeom, P.P.G. Guimaraes, H.M. Ahn, B.K. Jung, Q. Hu, K. McHugh, M.J. Mitchell, C.O. Yun, R. Langer, A. Jaklenec, *Adv. Mater.* 32 (2020), 1903878.
- J. Deng, S. Wu, M. Yao, C. Gao, *Sci. Rep.* 6 (2016) 31595.
- X. Zhao, S.Q. Zang, X. Chen, *Chem. Soc. Rev.* 49 (2020) 2481.
- S. He, C. Li, Q. Zhang, J. Ding, X.J. Liang, X. Chen, H. Xiao, X. Chen, D. Zhou, Y. Huang, *ACS Nano* 12 (2018) 7272.
- L. Wang, L. Zhu, M.T. Bernards, S. Chen, H. Sun, X. Guo, W. Xue, Y. Cui, D. Gao, *ACS Appl. Polym. Mater.* 2 (2019) 159.
- L. Kastl, D. Sasse, V. Wulf, R. Hartmann, J. Mircheski, C. Ranke, S. Carregal-Romero, J.A. Martinez-Lopez, R. Fernandez-Chacon, W.J. Parak, H.P. Elsasser, P. Riveria, *ACS Nano* 7 (2013) 6605.
- G. Sahay, E.V. Batrakova, A.V. Kabanov, *Bioconjugate Chem.* 10 (2008) 2023.
- X. Kang, Y. Yu, Z. Chen, Y. Wu, D. Wei, Y. Zhao, F. Wang, H. Xiao, *J. Mater. Chem. B Mater. Biol. Med.* 7 (2019) 3346.
- J. Huotari, A. Helenius, *EMBO J.* 30 (2011) 3481.
- L. He, Y. Li, C.P. Tan, R.R. Ye, M.H. Chen, J.J. Cao, L.N. Ji, Z.W. Mao, *Chem. Sci.* 6 (2015) 5409.
- M. Grossi, M. Morgunova, S. Cheung, D. Scholz, E. Conroy, M. Terrile, A. Panarella, J.C. Simpson, W.M. Gallagher, D.F. Oshea, *Nat. Commun.* 7 (2016) 1.
- Y. Tao, S. Liu, Y. Zhang, Z. Chi, J. Xu, *Polym. Chem.* 9 (2018) 878.
- G. Niu, P. Zhang, W. Liu, M. Wang, H. Zhang, J. Wu, L. Zhang, P. Wang, *Anal. Chem.* 89 (2017) 1922.
- D.J. Yang, L.Y. Lin, P.C. Huang, J.Y. Gao, J.L. Hong, *React. Funct. Polym.* 108 (2016) 47.
- Y. Jiang, N. Hadjichristidis, *Chin. J. Polym. Sci.* 37 (2019) 930.
- M. Nandi, B. Maiti, S. Banerjee, P. De, *J. Polym. Sci., Part A: Polym. Chem.* 57 (2019) 521.
- M. Hu, H.T. Feng, Y.X. Yuan, Y.S. Zheng, B.Z. Tang, *Coord. Chem. Rev.* 416 (2020), 213329.
- X. Hu, J. Hu, J. Tian, Z. Ge, G. Zhang, K. Luo, S. Liu, *J. Am. Chem. Soc.* 135 (2013) 17617.
- J. Xu, H. Chen, C. Yin, S. Lin, W.Y.-W. Lee, Y. Jing, Z. Li, Z. Yang, J. Xia, G. Chen, G. Li, L. Bian, *Nat. Commun.* 1 (2019) 2705.
- M. Xiong, M.W. Lee, R.A. Mansbach, Z. Song, Y. Bao, R.M. Peek, C. Yao, L.-F. Chen, A.L. Ferguson, G.C.L. Wong, *J. Chem. Proc. Natl. Acad. Sci.* 43 (2015) 13155.